Quantification of the Lateral Boundary Forcing of a Regional Climate Model Using an Aging Tracer

PHILIPPE LUCAS-PICHER

Danish Meteorological Institute, Copenhagen, Denmark, and Canadian Network for Regional Climate Modelling and Diagnostics, UQÀM, Montréal, Québec, Canada

DANIEL CAYA

Ouranos Consortium, and Canadian Network for Regional Climate Modelling and Diagnostics, UQÀM, Montréal, Québec, Canada

SÉBASTIEN BINER

Ouranos Consortium, Montréal, Québec, Canada

RENÉ LAPRISE

Canadian Network for Regional Climate Modelling and Diagnostics, UQÀM, Montréal, Québec, Canada

(Manuscript received 1 November 2007, in final form 14 April 2008)

ABSTRACT

The present work introduces a new and useful tool to quantify the lateral boundary forcing of a regional climate model (RCM). This tool, an aging tracer, computes the time the air parcels spend inside the limited-area domain of an RCM. The aging tracers are initialized to zero when the air parcels enter the domain and grow older during their migrations through the domain with each time step in the integration of the model. This technique was employed in a 10-member ensemble of 10-yr (1980–89) simulations with the Canadian RCM on a large domain covering North America. The residency time is treated and archived as the other simulated meteorological variables, therefore allowing computation of its climate diagnostics. These diagnostics show that the domain-averaged residency time is shorter in winter than in summer as a result of the faster winter atmospheric circulation. The residency time decreases with increasing height above the surface because of the faster atmospheric circulation at high levels dominated by the jet stream. Within the domain, the residency time increases from west to east according to the transportation of the aging tracer with the westerly general atmospheric circulation. A linear relation is found between the spatial distribution of the internal variability—computed with the variance between the ensemble members—and residency time. This relation indicates that the residency time can be used as a quantitative indicator to estimate the level of control exerted by the lateral boundary conditions on the RCM simulations.

1. Introduction

Regional climate models (RCMs) have been widely used for more than 15 yr to simulate climate at the regional scale (Giorgi 1990). RCMs allow climate simulations with high spatial resolutions that are not accessible with general circulation models (GCMs) or objective reanalyses (RAs). The RCM approach consists of using a fine-resolution grid over a limited-area domain, which requires to be fed at its boundaries by large-scale information usually taken from a GCM or RA. Initial studies conducted in the early 1990s demonstrated that this technique satisfies the fundamental principles defining RCMs (Dickinson et al. 1989; Giorgi 1990; Jones et al. 1995, 1997). More recently, RCMs were successfully validated by experimental observations and further refined by coupling the atmospheric models with sophisticated soil parameterizations and regional ocean models (see reviews by McGregor 1997; Houghton et al. 1996, 2001; Solomon et al. 2007). RCMs climate change projections are now used by the impact and

Corresponding author address: Philippe Lucas-Picher, Danish Meteorological Institute, Lyngbyvej 100, DK-2100 Copenhagen E, Denmark.
E-mail: plp@dmi.dk

DOI: 10.1175/2008MWR2448.1

adaptation community to anticipate the regional impacts of climate changes and to help in decision-making processes (Solomon et al. 2007). Regional climate change projections require climate modelers to give the most reliable projections and information about the associated uncertainties. In this perspective, many intercomparison projects of RCMs have been recently undertaken [e.g., Prediction of Regional Scenarios and Uncertainties for Defining European Climate Change Risks and Effects (PRUDENCE; Christensen et al. 2002), the Project to Intercompare Regional Climate Simulations (PIRCS; Takle et al. 1999), the North American Regional Climate Change Assessment Program (NARCCAP; Mearns 2004), and the Arctic Region Model Intercomparison Project (ARCMIP; Tjernstrom et al. 2005)].

As GCMs, the uncertainties in RCMs come from many sources: the emission scenarios, imperfections in model formulation, the parameterization used to define processes at scales not resolved by the RCM, and the internal variability (IV) of the simulated climate system. However, RCMs have an additional source of uncertainty, which comes from the lateral boundaries information, to which they are directly indebted (Noguer et al. 1998; Vidale et al. 2003; Wu et al. 2005). As GCMs, RCMs are also chaotic in their nature since they are built on the physical laws describing the behavior of a chaotic system. Therefore, different solutions can emerge from an ensemble of RCM simulations launched with slightly perturbed initial conditions, even if the RCM simulations are constrained by the same large-scale information at the boundaries (Giorgi and Bi 2000; Weisse et al. 2000; Christensen et al. 2001; Caya and Biner 2004; Rinke et al. 2004; Alexandru et al. 2007; de Elía et al. 2008; Lucas-Picher et al. 2008).

However, the predictability of an RCM is different from that of a GCM. Due to the chaotic nature of the atmospheric flow, the deterministic predictability period in a GCM simulation is limited to about two weeks. This means that two GCM simulations started with small differences in their initial condition will become totally uncorrelated after about two weeks. In an RCM, two simulations started with different initial conditions will also diverge with time and evolve differently from one another. However, these simulations will keep a certain level of correlation throughout the simulation because they share the lateral boundary forcing. For this reason, the predictability of an RCM is sometimes termed "extended" (Anthes et al. 1985; Laprise et al. 2000; de Elía et al. 2002) relative to that of a GCM. On some occasions, this extended predictability is temporarily lost in RCMs. Indeed, a phenomenon, identified as intermittent divergence in phase space (IDPS; von Storch 2005a, b), occurs when different trajectories emerge from an ensemble of RCM simulations initialized by slightly different initial conditions and driven by the same set of lateral boundary conditions (LBCs). The hypothesis is that the RCM tendency to exhibit IDPS depends on the intensity of the "flushing regime" of the limited-area domain by the atmospheric flow (i.e., the time needed for an air parcel to travel from the inflow to the outflow boundary). The flushing regime is governed by the atmospheric circulation, which depends on the synoptic conditions. It is thought to be an indicator of the efficiency of the steering exerted by the LBC on the RCM (von Storch 2005b). The IDPS phenomenon is intermittent and the simulations converge back when the influence of the LBC on the RCM recovers following a favorable atmospheric circulation. The large variability of solutions for the same LBC in the presence of IDPS renders impossible the deterministic time-by-time comparison of RCMs' simulations nested by RA with observations (Laprise 2005).

Moreover, the control exerted by the LBC on the RCM simulation, which restricts the RCM's IV, depends on the location of the domain (Rinke et al. 2004), the size of the domain (Jones et al. 1995; Jacob and Podzun 1997; Christensen et al. 2001; Vannitsem and Chomé 2005), the season (Noguer et al. 1998; Giorgi and Bi 2000; Caya and Biner 2004) and the synoptic conditions within the limited-area domain (Giorgi and Bi 2000). When the limited-area domain of an RCM is large, the lateral boundary forcing on the simulation is weaker and the RCM develops its own large scales apart from the one of the driving field (Jones et al. 1995; Jacob and Podzun 1997; Vannitsem and Chomé 2005). For example, Miguez-Macho et al. (2004) observed that the monthly-mean spatial distribution of precipitation, using the Regional Atmospheric Modeling System (RAMS) over a large domain covering North America, is modified when the domain is slightly moved. They explained this behavior by the distortion of the large-scale circulation produced by the interaction of the large scales generated by the RCM with those present in the LBC of the nested domain.

A strong zonal circulation responding to the strong temperature and pressure gradients characterizes midlatitude RCM's domains, such as those used in Europe and North America. This fast circulation continually forces new information from the driving field into the domain and sweeps away the internally generated model solution (Rinke et al. 2004). However, RCM domains centered over the Arctic are characterized by a weaker circulation through their lateral boundaries and the predominantly axisymmetric vortex impedes rapid migration of a given perturbation out of the domain

(Rinke et al. 2004). Therefore, a perturbation stays longer in a limited-area domain over the Arctic than in a midlatitude domain, allowing more time for the RCM to diverge from the solution of the large-scale driving fields (Rinke and Dethloff 2000).

Many studies have shown that the RCM's IV is seasonally dependent. Giorgi and Bi (2000) mentioned that the IV is larger in summer due to the moist convection activity and the local processes that are maximum in summer. These factors add a strong element of randomness and nonlinearity to the model, which maximize the IV in summer. Caya and Biner (2004), who also observed larger IV in summer, suggested that the control from the LBC in summer is not able to overcome the IV of the model. Rinke et al. (2004) obtained a different annual cycle of the RCM IV over the Arctic with larger values in autumn and winter. They explained this different behavior with the polar vortex observed in autumn and winter, which forces perturbations to stay into the domain.

In an ensemble of RCM simulations, Separovic et al. (2008) found high reproducibility of the large-scale circulation in the upper atmosphere. The lowest reproducibility was found near the surface and has been linked to a probable large residency time of the air parcels close to the surface. They also noted that the large-scale transient eddies are completely reproducible at the inflow boundary and the reproducibility decreases moving toward the outflow boundary. Leduc and Laprise (2008) showed that a "spatial spinup" is required to allow the complete development of the small scales and noticed that this spinup increases with faster atmospheric circulations at higher levels. Lucas-Picher et al. (2008) found that IV generally increases from west to east within their North American domain according to the general atmospheric circulation that usually forces new information in the domain through the western boundary. They also identified the largest IV in the northeast of the domain near the outflow boundary.

In all the above-mentioned studies, there appears to be a link between the IV and the control exerted by the LBC. This control appears to be associated to the so-called flushing regime that is dependent of the size of the domain, its geographical location, and the strength of the atmospheric circulation. All these characteristics have been reported in a more or less qualitative way so far: the limited-area domain is "small" or "large," the atmospheric circulation is "stronger" in winter than in summer, midlatitude domains show "less" IV than circumpolar ones, etc.

The present work introduces, for the first time, a method to quantify the flushing regime as an indicator of the forcing of the LBC on the RCM for a given configuration. This method uses aging tracers, which measure the time that air parcels spend within the limited-area domain of an RCM. This residency time is archived as the other model variables and can, therefore, be diagnosed as any other archived parameters (e.g., the climatology of the residency time can be computed). Thereafter, the amount of time spent by the air parcels within the domain can be assessed in space and time. We present a link between the residency time and the RCM's IV. A straightforward application of this association will be to use the residency time as a tool to quantify the control exerted by the LBC on the RCM simulation. At the same time, this study validates the current notion that the IV is dependent of the lateral boundary control determined by the atmospheric circulation (Rinke et al. 2004; von Storch 2005a,b; Lucas-Picher et al. 2008).

The next section describes the experimental setup: the RCM used, the ensemble of simulations, and the functioning of the aging tracer. The climate diagnostics of the residency time is presented in section 3 while a link between the residency time and the RCM's IV is examined in section 4. Finally, discussions and conclusions complete the document in section 5.

2. Experimental setup

a. The Canadian Regional Climate Model

The Canadian Regional Climate Model (CRCM; Caya and Laprise 1999) was used to generate the ensemble of simulations required for the computation of the IV and of the residency time. The CRCM uses a semi-implicit, semi-Lagrangian marching scheme to solve the time integration of the fully elastic nonhydrostatic Euler equations. The model's horizontal grid is polar stereographic with a 45-km grid mesh (true at 60°N). This study uses the version 3.7 of the CRCM as described in Plummer et al. (2006).

b. The ensemble of simulations

The ensemble of simulations used in this study is the same as in Lucas-Picher et al. (2008). It consists of 10 simulations of 10 yr (1980–89) over a domain that covers most of North America (Fig. 1). The domain contains 193 × 145 grid cells in the horizontal and 29 Gal-Chen levels in the vertical. Despite the large size of the domain, no large-scale nudging was applied in order to retain the IV generated by the RCM over this domain. To construct the ensemble, simulations were launched with different initial conditions obtained by lagging the start of the simulations or by adding small random perturbations. The source of the perturbations has no in-

FIG. 1. North American domain used for the CRCM ensemble simulations. This domain contains 193 × 145 grid cells at 45-km resolution. The region indicated by the inner dotted square represents the computationally free domain. Topographic heights are contoured at every 500 m.

fluence on the IV 15 days after the beginning of the simulation (Giorgi and Bi 2000; Lucas-Picher et al. 2008).

The lateral boundary and the initial atmospheric state (i.e., horizontal winds, vertical motion, temperature, pressure, and specific humidity) come from the National Centers for Environmental Prediction–National Center for Atmospheric Research (NCEP–NCAR) reanalysis data (resolution: 2.5° × 2.5° on 28 levels; Kalnay et al. 1996). The atmospheric fields feed the limited-area domain every 6 h and linear interpolation in time is made to generate the driving fields required at each 900-s time step. At the lateral boundaries, the nudging scheme of Davies (1976) is applied on the horizontal winds over a relaxation zone of nine grid points. The relaxation zone is removed for all diagnostics. The initial conditions for the land surface variables (i.e., surface temperature, liquid and frozen soil water fraction, snow amount, and snow age) are taken from a 1° × 1° climatology of the Canadian GCM version 2 (GCM2; McFarlane et al. 1992). Finally, the sea surface temperature (SST) and sea ice distribution are obtained from the 1° × 1° Atmospheric Model Intercomparison Project (AMIP) monthly means (Gates et al. 1999).

c. *The aging tracer*

The concept behind the aging tracer is to compute the time since the air parcels enter the RCM domain. It works in a similar way as a passive tracer that computes the concentration of a pollutant, but the concentration is replaced by the residency time. At the inflow boundary, an aging tracer initialized to zero is attributed to each air parcel that enters the domain. Then, the tracer grows older at every time step of the CRCM model during its migration through the domain following the atmospheric circulation. The aging tracer is advected and diffused by the atmospheric flow simulated with the CRCM dynamics equations. The tracer is also interpolated through the semi-Lagrangian numerical scheme and the time filter, which control the rapid oscillations generated by the numerical scheme. The trajectory of a specific air parcel cannot be tracked using this approach. The value of the residency time of a grid point corresponds to the "average age" of the parcel over the air volume that covers the grid point in the three-dimensional grid. The aging tracer is not treated by the physical parameterization of the model (such as the convection), but it can move vertically by the resolved vertical motion of the CRCM dynamics. The vertical transport by convection is expected to be negligible compared to horizontal transport for time scales addressed in the analysis. The residency time is treated and archived as any other simulated meteorological variable, therefore allowing computation of its climate diagnostics.

Similarly, Gheusi and Stein (2002) studied the flow dynamic in an atmospheric model with three Eulerian passive tracers initialized with the spatial coordinates of each grid cell. In their study, the tracers within the airflow experience the transport processes: advection, subgrid turbulence, and convective transport. This method allows the identification of each Lagrangian air parcel by referring to its initial location. The physical history of each air parcel can thus be retrieved to characterize the atmospheric circulation. While the residency time is not explicitly calculated by this method, it can be estimated by computing the time a parcel takes to move from its initial to its final position.

3. Residency time diagnostics

a. *Instantaneous values of the residency time*

A first insight into the residency time field was obtained by snapshots of the ensemble mean at different heights (Fig. 2). The first column of Fig. 2 shows a summer case at 0000 UTC 30 June 1980 where the flushing regime is weaker. At 200 hPa (Fig. 2a), there are large meanders in the atmospheric circulation, which maintains the air parcels within the domain for extended periods of time. Values of residency time reaching 10 days are observed in the northern part of the domain. At the lower levels, the atmospheric circulation is generally slower, thus increasing the residency

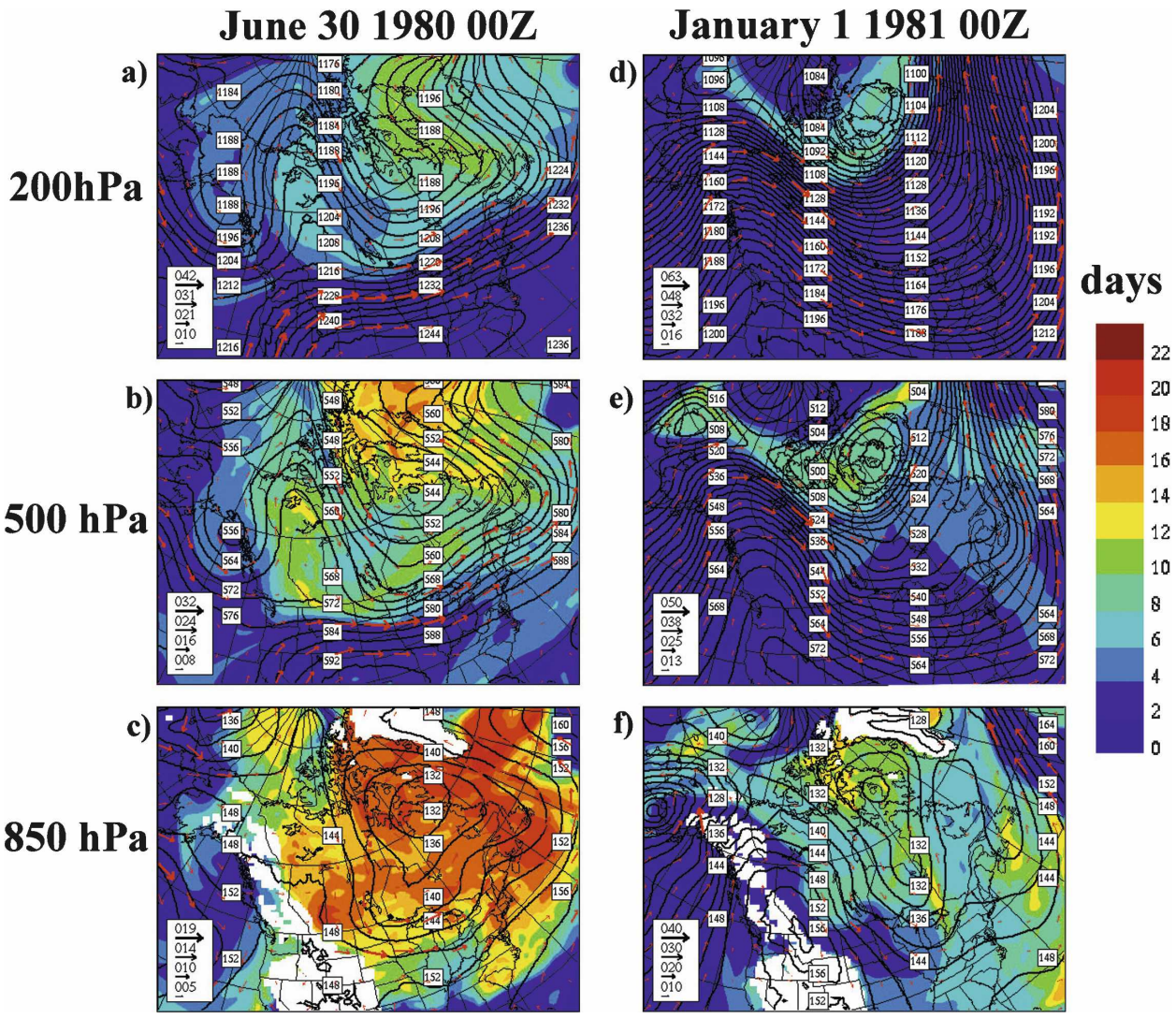

FIG. 2. Residency time (colors), geopotential height (black contours), and wind vector (red arrows) of the ensemble mean at 0000 UTC 30 Jun 1980 at (a) 200, (b) 500, and (c) 850 hPa. (d), (e), (f) Respective fields are repeated for 0000 UTC 1 Jan 1981. The color scale indicates the residency time in days, the labels describe the black contours geopotential heights in dekameters, and the length of the arrows indicate the wind velocity in meters per second with different scales for each figure. A white mask is used to remove the residency time values where the land surface crosses the 850-hPa level.

time. At 500 and 850 hPa (Figs. 2b,c), a low pressure system located at the center of the domain keeps the air parcels inside the domain. At 850 hPa, the residency time is close to 15 days all over the domain, except near to the boundaries.

The second column of Fig. 2 shows a winter case at 0000 UTC 1 January 1981 with a stronger flushing regime and smaller values of residency time than for previous summer snapshot. The strong gradient of geopotential heights generates a fast zonal atmospheric circulation at 200 hPa that quickly transports the aging tracer out of the domain, resulting in small values of residency time (Fig. 2d). Only a small region in the north of the domain has residency times longer than 2 days. A fast atmospheric circulation travels through the domain and crosses the boundaries, which increases the flow of young air parcels entering, and old air parcels leaving, the domain. At 500 and 850 hPa (Figs. 2e,f), the residency time is larger than at 200 hPa because of the slower atmospheric circulation, reaching values between 8 and 12 days at 850 hPa (Fig. 2f).

In Figs. 2c,f, a mask identifies the regions where the land surface crosses the 850-hPa level. In these regions, a simple extrapolation from the first level of the terrain-following coordinate is done to compute the values of the variable under the land surface. This procedure al-

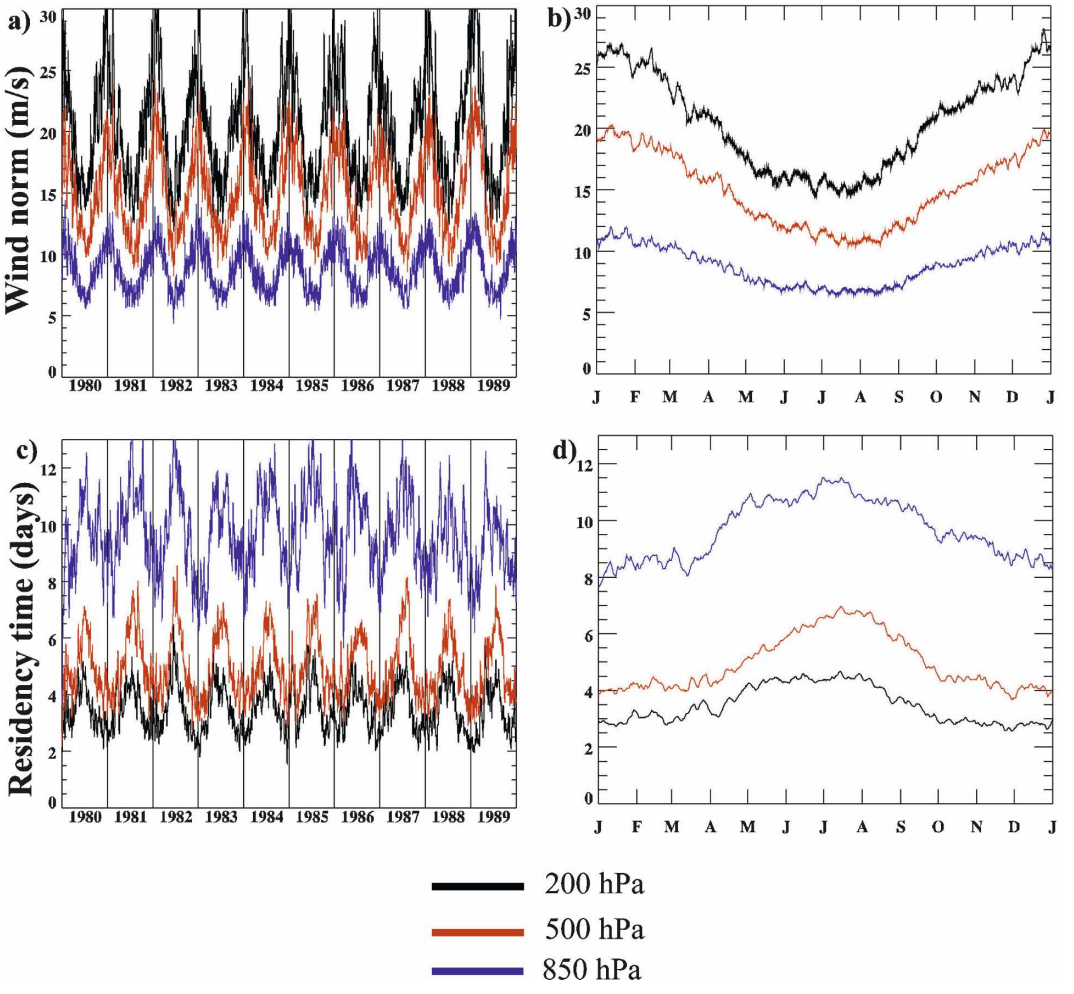

FIG. 3. (a) 1980–89 times series and (b) mean annual cycle of the ensemble mean for the domain-averaged wind norm (m s^{-1}) at 200, 500, and 850 hPa. (c), (d) As in (a), (b), but for the residency time (days).

lows the definition of continuous fields, but values in these regions are sometimes affected by this treatment. The resulting field gives a false representation of the residency time, which explains why the residency time values are masked over these regions. However, the wind and the geopotential heights are not masked and, therefore, must be interpreted with caution in these regions.

b. *Evolution of the residency time*

Figure 3 shows the 1980–89 time series and mean annual cycles of the ensemble mean for the wind norm $\|\mathbf{X}\|$ and for the residency time at 200, 500, and 850 hPa. The wind norm is computed as

$$\|\mathbf{X}\| = \sqrt{u^2 + v^2}, \tag{1}$$

where u and v are the horizontal components of the wind vector. In summer, the domain-averaged atmospheric circulation is twice as fast at 200 hPa (15 m s^{-1}) than at 850 hPa (7 m s^{-1}; Fig. 3b). Consequently, the air parcels travel faster from the inflow boundary to the outflow boundary in the higher levels, and remain in the domain for a shorter period of time. The associated residency time of the air parcels is smaller at 200 hPa (4 days) than at 850 hPa (11 days; Fig. 3d). Between 200 and 850 hPa, the atmospheric circulation is twice as fast but is 3 times shorter for residency time because of the more zonal circulation at the higher levels. In winter, all levels exhibit faster wind circulation and shorter residency time compared to the summer season.

c. *Spatial distribution of the mean residency time*

Figure 4 presents the 1980–89 summer and winter climatology of the ensemble-mean residency time, geopotential heights, and wind vectors at 200, 500, and 850 hPa, respectively, thus allowing a clear identification of

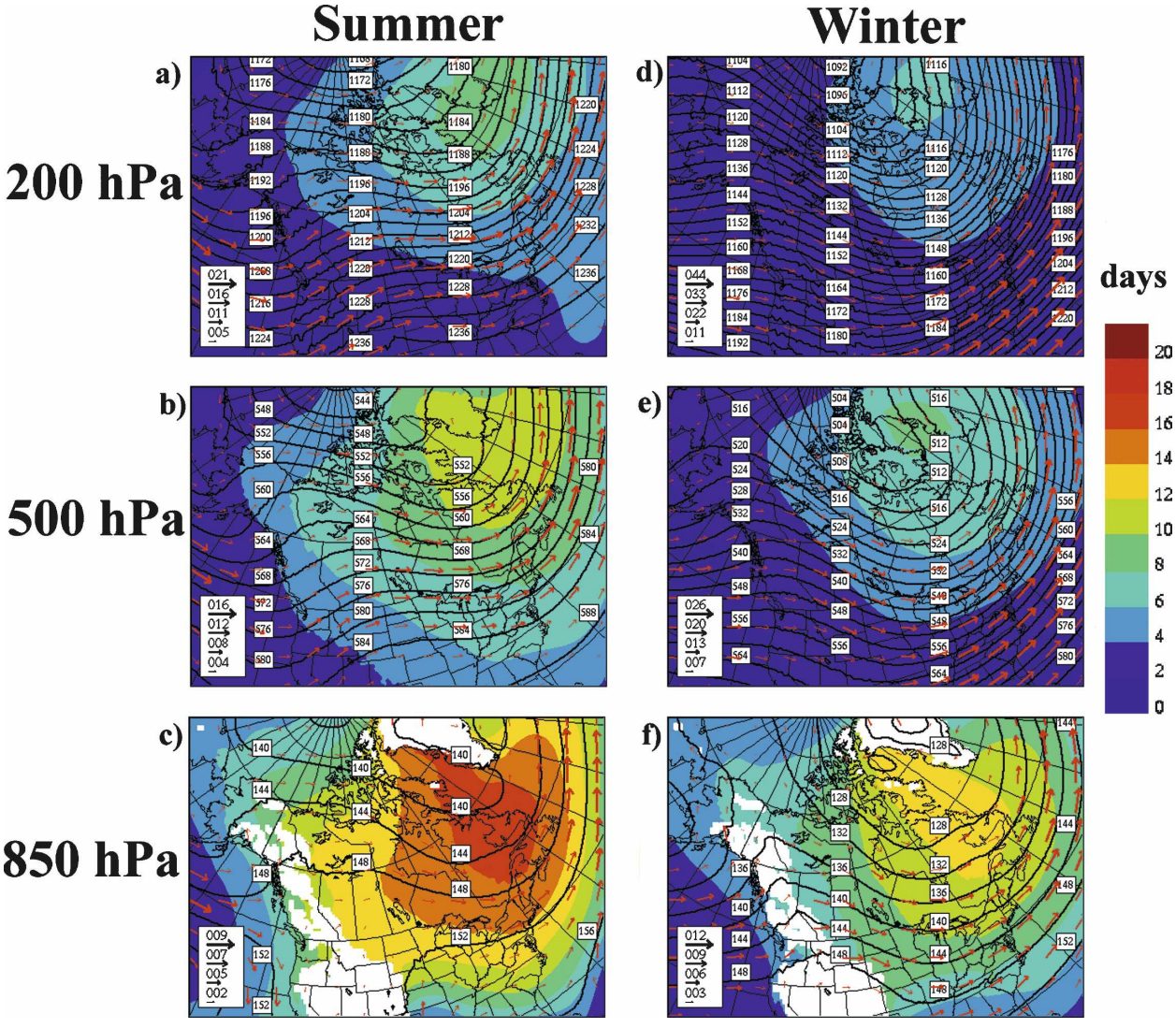

FIG. 4. 1980–89 ensemble-mean residency time (colors), geopotential heights (black contours), and mean wind vector (red arrows) in summer (JJA) at (a) 200, (b) 500, and (c) 850 hPa. (d), (e), (f) Respective fields for winter season (DJF) are shown. The color scale indicates the residency time in days, the labels describe the black contours geopotential heights in dekameters, and the length of the arrows indicates the wind velocity in meters per second with different scales for each figure. A white mask is used to remove the residency time values where the land surface crosses the 850-hPa level.

the mean inflow and outflow boundaries. The small values of the residency time and the incoming wind vectors on the western side of the domain identify the mean inflow boundary, while the large values of the residency time and the outgoing wind vectors in the northeast of the domain identify the mean outflow boundary. Generally, the residency time increases from west to east because of the aging of the tracer during its migration toward the east following the westerly general atmospheric circulation. We can also see that the residency time is shorter in winter and than in summer because of the faster atmospheric circulation in winter. Furthermore, the residency time decreases with increasing height according to the faster atmospheric circulation in higher levels.

At 200 and 500 hPa, the longest residency time in both seasons is located over Greenland, and is associated to the outflow boundary of the atmospheric circulation. At 850 hPa, the atmospheric circulation is less zonal than at 200 hPa, and is affected by the traveling low and high pressure systems, explaining why the longest residency times at 850 hPa are located over the north of Québec, Canada, away from the boundaries. At the mean outflow boundary, the atmospheric circulation is such that, occasionally, the atmospheric flow changes direction and enters the domain from that

boundary. Therefore, the mean residency time computed close to each boundary of the domain is close to zero (not shown because the nine-gridpoint sponge zone is removed from the graph).

4. Link between the residency time and the internal variability

Rinke et al. (2004) mentioned that the RCM IV is generally larger in domains covering the Arctic than in the midlatitudes, following the general atmospheric circulation characterizing those regions. Von Storch (2005b) proposed that the level of variability of the RCM solutions for a certain set of LBC is associated to the flushing regime of a limited-area domain. Similarly, Lucas-Picher et al. (2008) associated the spatial distribution of the IV to the general atmospheric circulation. These studies support the hypothesis that the RCM IV is related to the control of the LBC (conditioned by the atmospheric circulation) on the RCM simulation. The next section describes the diagnostics of the IV from an ensemble of simulations. Then, the IV will be compared to the residency time in order to identify relations between these fields and to verify the previously stated hypothesis.

a. Diagnostics of the internal variability

The procedure described in Lucas-Picher et al. (2008) defines the IV as the intermember variance σ_X^2:

$$\sigma_X^2(i,j,k,t) = \frac{1}{M-1}\sum_{m=1}^{M}[X(i,j,k,t,m) - \langle X\rangle(i,j,k,t)]^2, \tag{2}$$

where $X(i, j, k, t, m)$ refers to the value of the climate parameter X at coordinate (i, j, k) in the three-dimension grid at the archival time t for member m of the M-member ensemble. The term $\langle X\rangle(i, j, k, t)$ is the ensemble mean defined as

$$\langle X\rangle(i,j,k,t) = \frac{1}{M}\sum_{m=1}^{M} X(i,j,k,t,m). \tag{3}$$

The evolution of the IV is computed using domain-averaged values as

$$\overline{\sigma_X^2}^{xy}(k,t) = \frac{1}{I\times J}\sum_{i=1}^{I}\sum_{j=1}^{J}\sigma_X^2(i,j,k,t), \tag{4}$$

where I and J are the number of grid cells along the horizontal plane over the domain of interest (excluding the relaxation zone).

To describe the spatial distribution of the IV, the climatology of the IV is computed with the time average of σ_X^2 defined as

$$\overline{\sigma_X^2}^{t}(i,j,k) = \frac{1}{N}\sum_{t=1}^{N}\sigma_X^2(i,j,k,t), \tag{5}$$

with N as the number of archived time steps over the period of interest.

As explained in Lucas-Picher et al. (2008), two factors contribute to the internal variability. The first factor is related to the temporal decorrelation between the members of the ensemble, which depends on the strength of the lateral boundary forcing on the RCM simulations. At the boundary inflow, the information from the driving fields enters the RCM domain, therefore in this region, the RCM simulations are forced by the driving field and simulations follow a similar path resulting in a weak IV (low intermember variance). As the air parcels move away from the inflow boundary, the lateral boundary forcing weakens and the chaotic nature of the atmospheric flow tends to decorrelate the circulations between members of the ensemble, this increasing the IV (higher intermember variance). The IV usually reaches its maximum near the outflow boundary. The second factor arises from the temporal variability σ_t (also known as the climate or natural variability; Caya and Biner 2004; Lucas-Picher et al. 2008). The maximum of IV computed with the intermember variance of a large ensemble of regional simulations is equal to the temporal variance σ_t^2 when the members of the ensemble are completely uncorrelated and unbiased. The temporal variance also corresponds to the GCM's IV where simulations become uncorrelated after a few weeks of simulation. The temporal variance σ_t^2 is computed as

$$\sigma_t^2(i,j,k,m) = \frac{1}{N-1}\sum_{t=1}^{N}[X(i,j,k,t,m) - \overline{X(i,j,k,m)}^{t}]^2, \tag{6}$$

where the $^{-t}$ operator refers to a time average and N is the number of archived time steps over the period of interest. The ensemble mean of σ_t^2 can be computed as

$$\overline{\sigma_t^2}^{m}(i,j,k) = \frac{1}{M}\sum_{m=1}^{M}\sigma_t^2(i,j,k,m). \tag{7}$$

Thus, as described in Lucas-Picher et al. (2008), to remove the portion of the IV due to the temporal variance in the analysis, the IV computed as the intermember variance σ_X^2 [hereinafter described by the absolute internal variability (AIV)] can be normalized by the temporal variance σ_t^2 to obtain the relative internal variability (RIV). The latter varies between 0 and 1. An

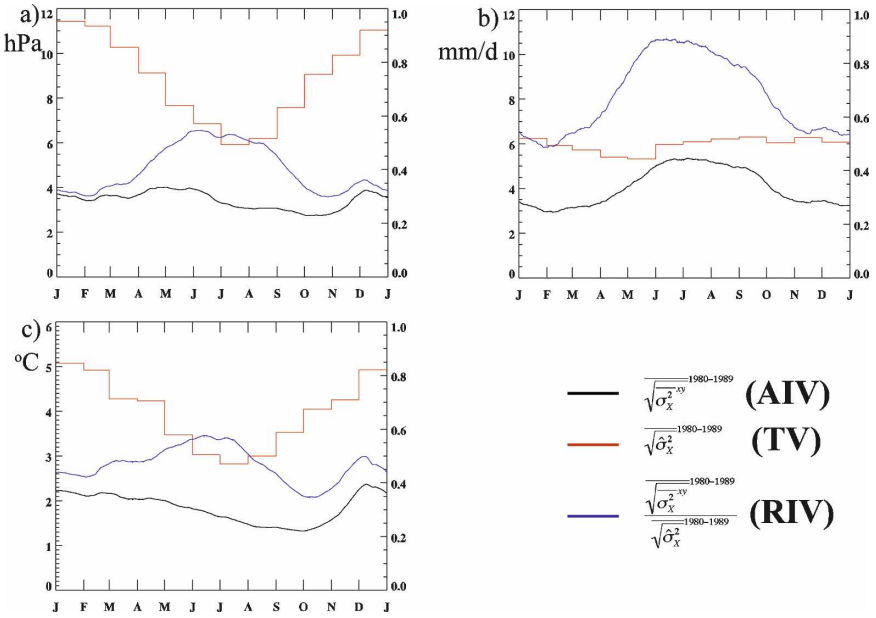

FIG. 5. Mean-annual cycle of the AIV (black), TV (red), and RIV (blue) over 1980–89 for (a) MSLP (hPa), (b) PCP (mm day^{-1}), and (c) ST (°C). The mean annual cycle of the TV of the first member is presented. The values of the AIV and TV are associated to the left-hand-side scale while the values of the RIV are associated to the right-hand-side scale. A 30-day moving average is applied to the values of the AIV and RIV.

RIV of 0 means that there is no internal variability, that simulations are perfectly correlated, and that the lateral boundary forcing is strong. At the opposite, an RIV of 1 means that the internal variability is at its maximum, that simulations are uncorrelated, and that the lateral boundary forcing is too weak to have any control on the simulation, making the RCM behave as a GCM.

To compute the evolution of the RIV, Lucas-Picher et al. (2008) normalized the domain-averaged inter-member variance (AIV) with the domain-averaged monthly temporal variance $\hat{\sigma}_X^2$ (Caya and Biner 2004) computed as

$$\hat{\sigma}_X^2(i,j,k) = \overline{[X(i,j,k,t) - \overline{X(i,j,k)^t}]^2}^{xyt}, \qquad (8)$$

where the $^{-xyt}$ operator refers to a domain monthly time average and the $^{-t}$ operator refers to a monthly time average.

b. *Comparison between the evolution of the internal variability and the residency time*

The 1980–89 mean annual cycles of the AIV, RIV, and domain-averaged monthly temporal variance (TV) are presented in Fig. 5 for mean sea level pressure (MSLP), precipitation (PCP), and screen temperature (ST). The square root of the variance is used to recover the original units. The AIV of MSLP and ST displays a small annual cycle, with values slightly larger in winter and spring than in summer and fall. In contrast, the annual cycle of RIV for these parameters exhibits a large annual cycle with larger values in summer due to the normalization of the data against the monthly temporal variance, which is larger in winter than in summer. The large temporal variance in winter compared to summer for MSLP and ST is linked to the strong cyclonic activity that generates large low pressure systems in winter in the midlatitudes. For PCP, both AIV and RIV present a similar annual cycle with larger values in summer due to the small annual cycle of the monthly temporal variance. Contrary to the AIV, the mean annual cycles of the RIV for MSLP, ST, and PCP (Fig. 5) behave similarly to the mean annual cycle of the residency time (Fig. 3d). These findings support the fact that the RIV reduces the part of the IV due to the temporal variability and increases the part associated to the correlation between the simulations, which depends on the lateral boundary forcing that is linked to the atmospheric circulation. The larger values of the RIV in summer for each variable tell also that the simulations are less correlated from one another in summer than in winter because of the slower atmospheric circulation in summer, which reduces the lateral boundary forcing.

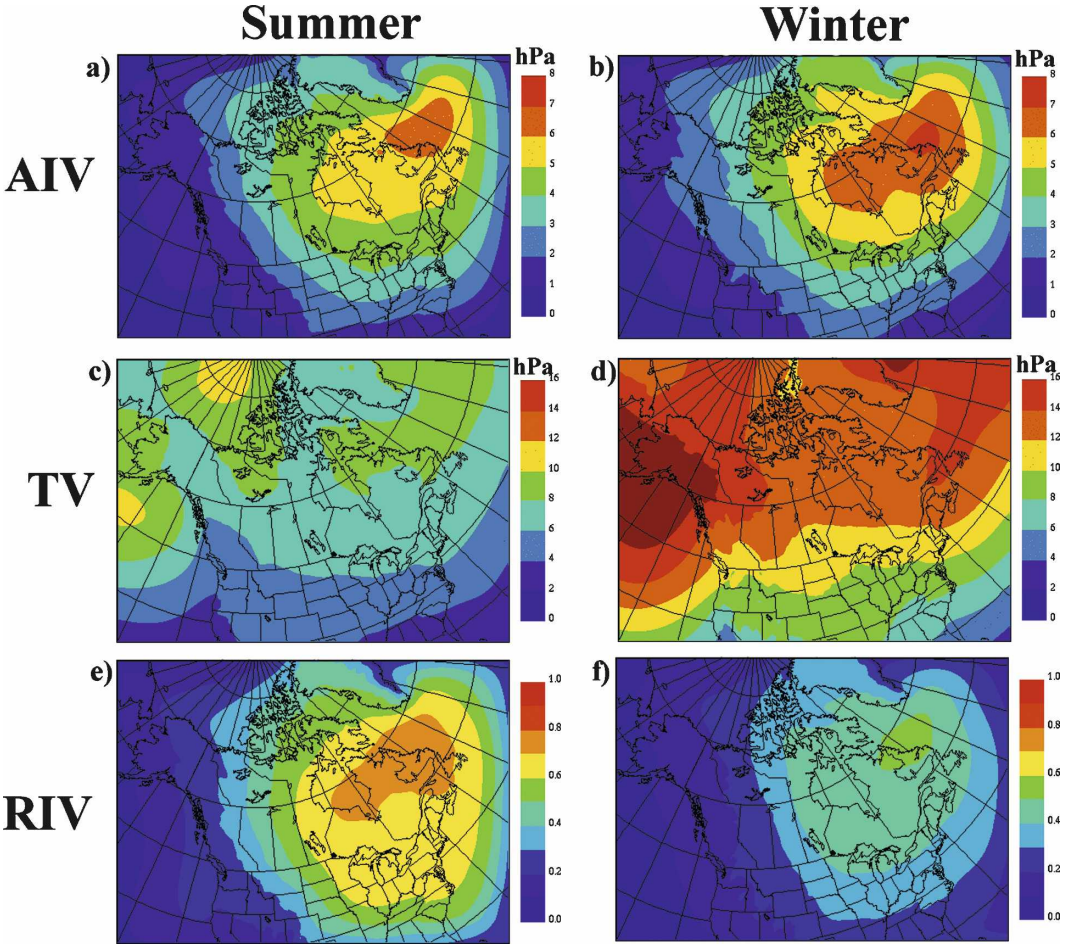

FIG. 6. AIV: Square root of the 1980–89 time-averaged intermember variance ($\sqrt{\overline{\sigma^2_{\text{mslp}}}^{\,t}}$) for MSLP in (a) summer and (b) winter. TV: Square root of the ensemble-mean temporal variance $\sqrt{\overline{\sigma_t^2}^{\,m}}$ from 1980 to 1989 in (c) summer and (d) winter. RIV: Ratio between (a), (b) $\sqrt{\overline{\sigma^2_{\text{mslp}}}^{\,t}}$ and (c), (d) $\sqrt{\overline{\sigma_t^2}^{\,m}}$ from 1980 to 1989 in (e) summer and (f) winter.

c. *Comparison between the spatial distribution of the internal variability and residency time*

Figures 6, 7, and 8 present the 1980–89 summer and winter spatial distributions of the AIV, TV, and RIV for MSLP, PCP, and ST, respectively. The spatial distribution of the AIV for MSLP is similar for each season, with larger values in the northeast of the domain (Figs. 6a,b). The temporal variance of MSLP is larger in winter (Fig. 6c) than in summer (Fig. 6d), with a south–north gradient. The resulting RIV (Figs. 6e,f) computed from the normalization of the AIV by the temporal variance (σ_t^2) is closer to 1 in summer than in winter, and larger values are located in the northeast of the domain. Lucas-Picher et al. (2008) reported that the RIV is related to the general atmospheric circulation and explained that the RIV is stronger near the outflow boundary in the northeast of the domain where the lateral boundary is weak. The larger values of the RIV in summer than in winter are explained by the weaker lateral boundary forcing in summer, which is related to the slower atmospheric circulation.

For PCP, the largest values of AIV are concentrated in the southeast region of the domain in summer (Fig. 7a) and on the east coast in winter (Fig. 7b). The temporal variance of PCP is similar to the AIV in summer (Fig. 7c), with larger values in the southeast of the United States, while it differs from the AIV in winter (Fig. 7d) with larger values on both the east and west coasts of North America. In summer, the RIV for PCP (Fig. 7e) is close to 1 in most parts of the domain, except close to the inflow boundary on the west side of the domain. In contrast, winter RIV values for PCP (Fig. 7f) are smaller than in summer, values close to 1

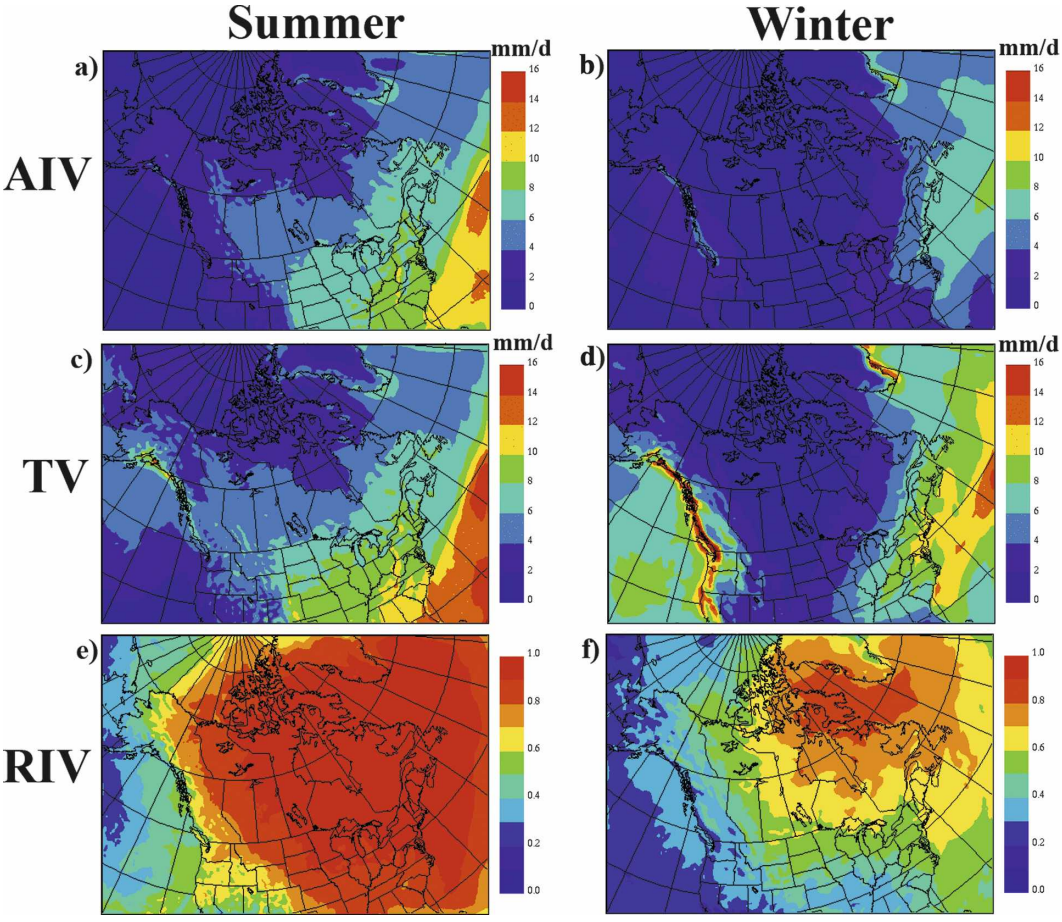

FIG. 7. As in Fig. 6, but for precipitation ($\sqrt{\overline{\sigma^2_{\text{pcp}}}^t}$) in (a) summer and (b) winter; $\sqrt{\overline{\sigma^2_t}^m}$ from 1980 to 1989 in (c) summer and (d) winter; and the ratio between (a), (b) $\sqrt{\overline{\sigma^2_{\text{pcp}}}^t}$ and (c), (d) $\sqrt{\overline{\sigma^2_t}^m}$ from 1980 to 1989 in (e) summer and (f) winter.

being located only in the northeast of the domain. These results suggest that the summer PCP is uncorrelated in each simulation and weakly conditioned by the driving field. Each simulation generates its own PCP, which responds to local forcing and depends weakly on the large-scale driving field. At the opposite, the winter values of RIV closer to 0 suggest that the lateral boundary forcing has a stronger influence on the generation of PCP in winter than in summer, probably due to the fast atmospheric circulation and the large low pressure systems. The use of the RIV removes the region dependence of the IV on PCP modulated by the temporal variability, and enhances the part of the internal variability related to the lateral boundary forcing and the atmospheric circulation. In the regions where the RIV is close to 1, the IV of the RCM is comparable to the one of a GCM, suggesting that the LBC does not contribute to the predictability of the RCM simulations.

For ST, large values of AIV are located south of the Hudson Bay in summer (Fig. 8a) while large values are located in the north of Canada in winter (Fig. 8b). The temporal variability for ST is larger in winter (Fig. 8c) than in summer (Fig. 8d). Finally, large values of RIV (between 0.5 and 0.7) are located over Québec in summer (Fig. 8e) and over the north of Canada in winter (Fig. 8f). While it cannot be seen in all figures because of the analysis performed in the free domain, the AIV and RIV decrease rapidly for all variables in the nine-gridpoint nudging zone (Davies 1976) to reach a null value at the boundary where the simulations must rejoin the driving field because of the one-way nesting.

The 1980–89 spatial distributions of the residency time at 850 hPa in summer (Fig. 4c) and winter (Fig. 4f) exhibit clear similarities with the spatial distribution of the AIV of MSLP in summer (Fig. 6a) and winter (Fig. 6b). To illustrate and quantify the relationship between these two variables, a scatter diagram linking the AIV and the residency time at 850 hPa is presented in Fig. 9.

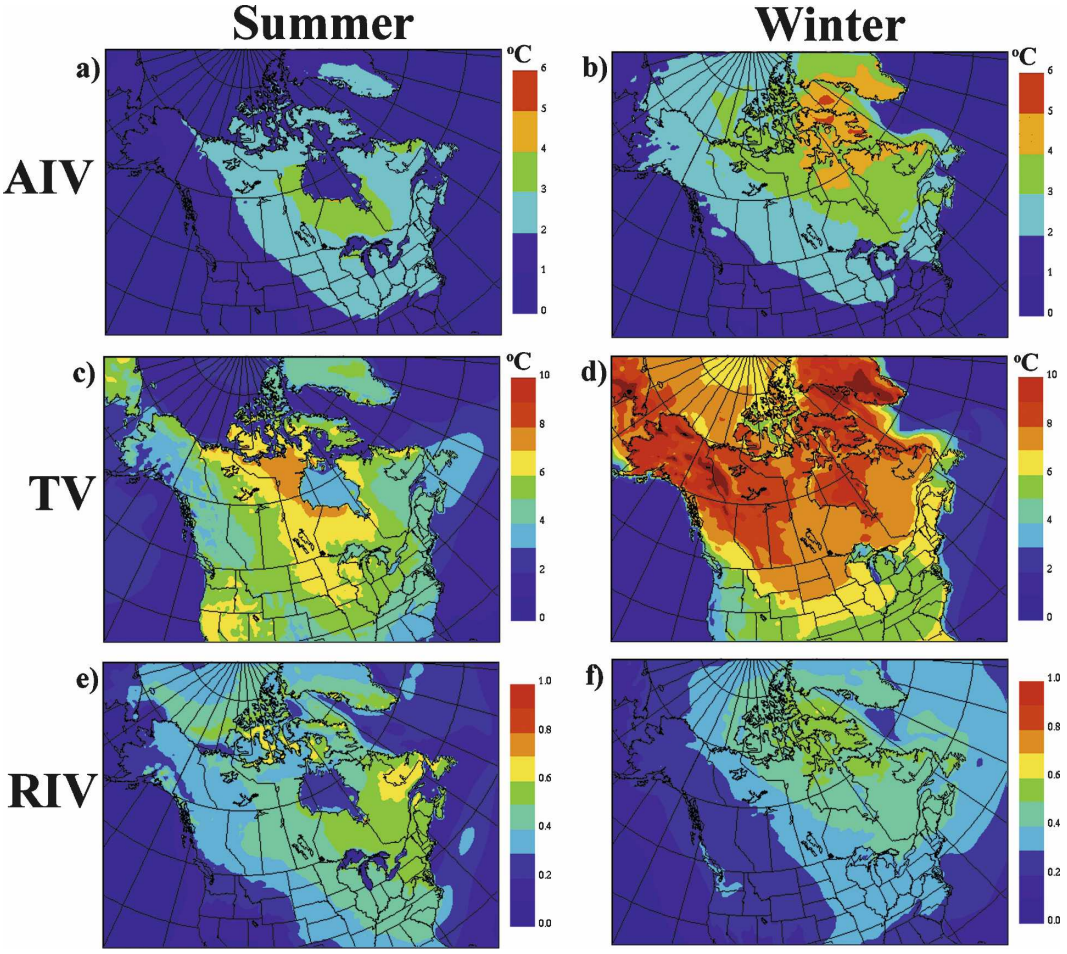

FIG. 8. As in Fig. 6, but for screen temperature ($\sqrt{\overline{\sigma_{\mathrm{st}}^{2\,t}}}$) in (a) summer and (b) winter; $\sqrt{\overline{\sigma_t^{2\,m}}}$ from 1980 to 1989 in (c) summer and (d) winter; and the ratio between (a), (b) $\sqrt{\overline{\sigma_{\mathrm{st}}^{2\,t}}}$ and (c), (d) $\sqrt{\overline{\sigma_t^{2\,m}}}$ from 1980 to 1989 in (e) summer and (f) winter.

Each dot in the scatter diagram represents the values of both variables for a given grid point in the free domain. The correlation, the best linear fit using a least squares method, and the number of grid points are also indicated in the diagrams. The residency time at 850 hPa was selected because this level allows appropriate comparison with the IV of the surface variables (MSLP, PCP, and ST) while minimizing the number of grid points under the land surface.

Figure 9a shows the scatter diagram of the 1980–89 time-averaged residency time at 850 hPa and AIV for mean sea level pressure in summer and in winter. There is a strong linear relation between the residency time and the AIV, with correlation coefficients >0.9 for both seasons. For a given residency time, the AIV is larger in winter than in summer and distinct data clouds are obtained for each season; the slope of the linear fit being larger in winter than in summer. Therefore, the AIV increases with residency time more rapidly in winter than in summer. According to the positive slope and the strong correlation coefficient, a general relation is identified, whereby the AIV increases linearly with the residency time. The same analysis for PCP (Fig. 9b) generated sparse overlapping data clouds for each season. The small correlation coefficients obtained for summer (0.34) and winter (0.26) indicate a weak relationship between the AIV for PCP and the residency time. Contrary to the residency time, the AIV for PCP is spatially related to the variability in PCP that falls in each region, thus explaining the sparse data cloud and the low correlation coefficients. For ST (Fig. 9c), the data clouds are separated for each season, and they contain fewer dots because of the mask over the ocean cells. These cells are removed from the analysis because they are highly conditioned by the imposed sea surface temperature, which restricts the variability between the

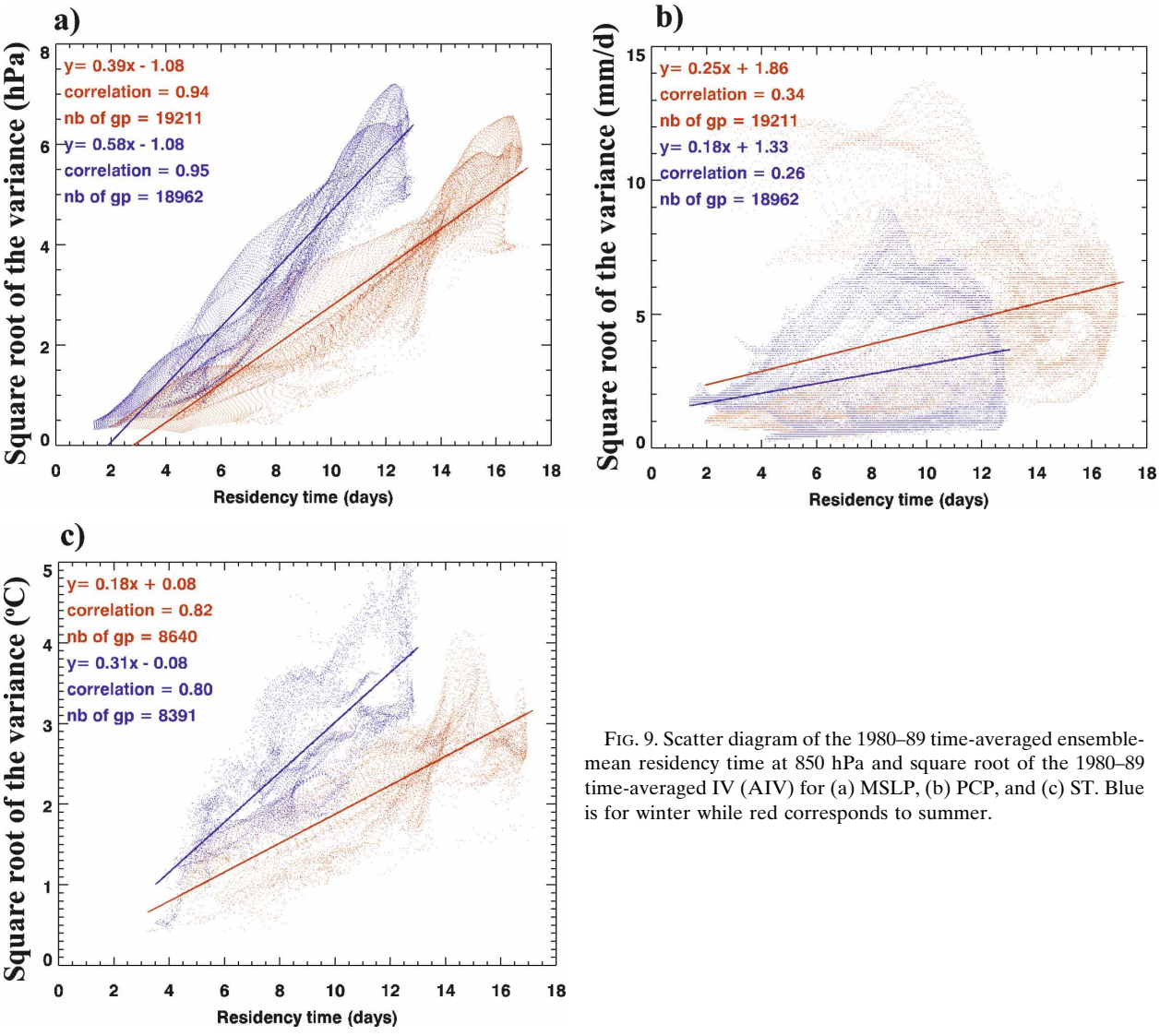

FIG. 9. Scatter diagram of the 1980–89 time-averaged ensemble-mean residency time at 850 hPa and square root of the 1980–89 time-averaged IV (AIV) for (a) MSLP, (b) PCP, and (c) ST. Blue is for winter while red corresponds to summer.

simulations. As for MSLP, the AIV increases linearly with the residency time. The linear correlation coefficients of 0.82 in summer and 0.80 in winter indicate a good relation between the residency time and the AIV for the screen temperature.

As previously mentioned, the use of the RIV reduces the part of the IV caused by the temporal variability, and increases the contribution of lateral boundary forcing and atmospheric circulation described by the residency time. To quantitatively determine the association between the RIV (Figs. 6, 7, and 8e,f) and the residency time (Figs. 4c,f), the scatter diagram analysis was repeated using the RIV instead of the AIV. Figure 10a shows that the data clouds generated for the summer and winter seasons using the RIV for MSLP are well mixed together, compared to the separated data clouds obtained by the analysis with the AIV (Fig. 9a). Linear fits for both seasons present similar correlation coefficients (0.92 in summer and 0.95 in winter) and slopes (0.05 in summer and 0.04 in winter). For PCP (Fig. 10b), the data clouds in winter and summer are also well mixed, except in summer for dots with residency time larger than 12 days where RIV values are close to 1. For those dots, the RIV has reached its maximum, meaning that the IV related to the residency time is maximum and that the simulations have lost all their predictability for the precipitation. Therefore, the use of the RIV reduced the spatial and seasonal dependences of the IV for PCP. It removes the part of the IV associated to the TV and shows that the contribution from the correlation term in the IV is related to the residency time, as shown by the merging of the summer and winter linear

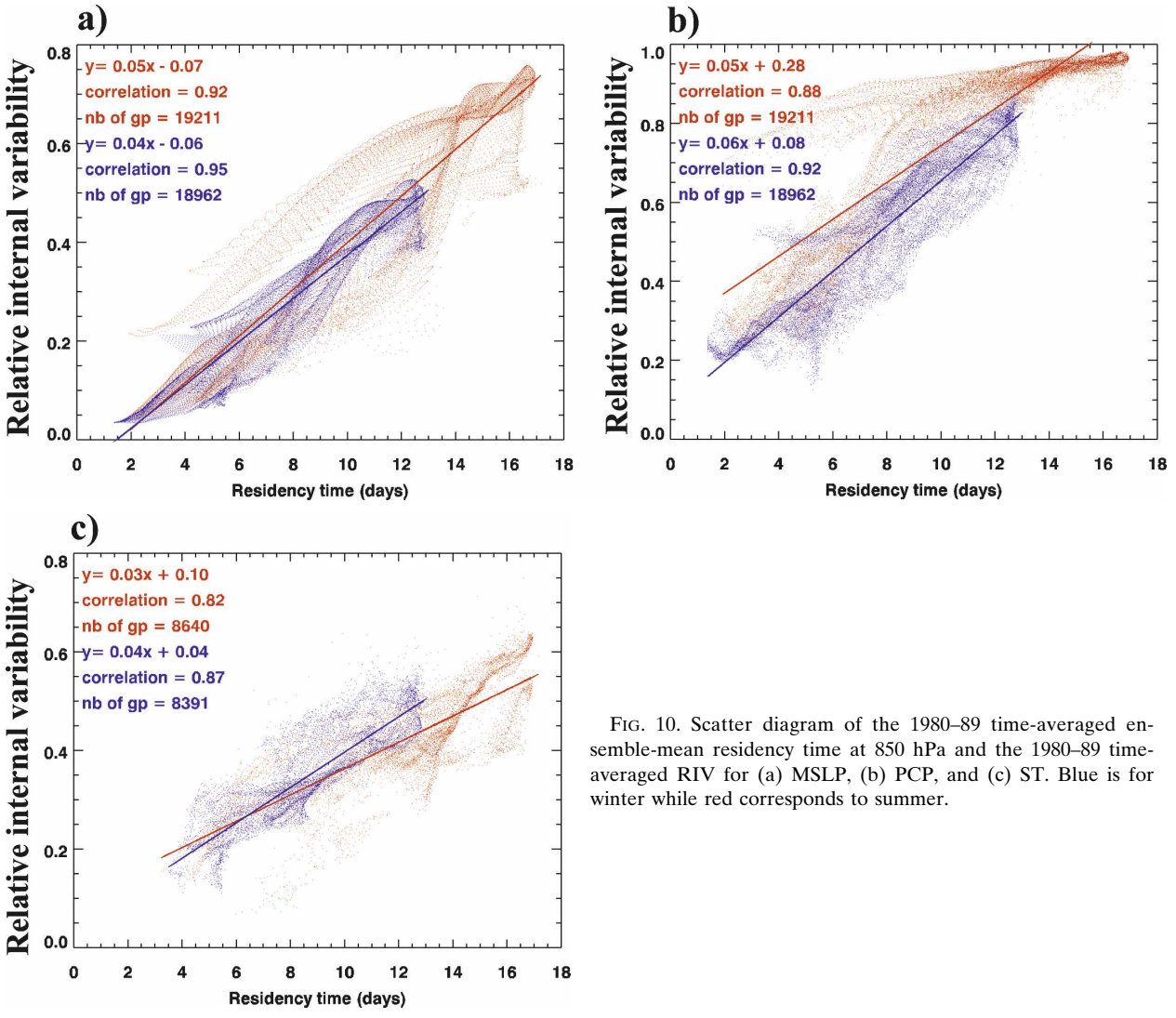

FIG. 10. Scatter diagram of the 1980–89 time-averaged ensemble-mean residency time at 850 hPa and the 1980–89 time-averaged RIV for (a) MSLP, (b) PCP, and (c) ST. Blue is for winter while red corresponds to summer.

fits. It also increases the correlation coefficients compared to those using the AIV in Fig. 9b. The scatter diagram for ST (Fig. 10c) is similar to the one of MSLP (Fig. 10a), where the data clouds are mixed together with similar large values of the correlation coefficients and similar slopes. In summary, for each variable, the use of the RIV rather than the AIV increases the correlation coefficients, especially for PCP, and merges together the data clouds of each season in the scatter diagram.

A general message arising from the presented scatter diagrams is that the RIV increases linearly at a similar rate in summer and winter with the residency time. Consequently, this analysis does not support the findings of Giorgi and Bi (2000) who used the convective activity and nonlinear processes to explain the larger IV in summer. However, this study supports the proposition that internal variability is associated to the control of the LBC linked to the atmospheric circulation that is described by the residency time (Caya and Biner 2004; Rinke et al. 2004; von Storch 2005b; Lucas-Picher et al. 2008). As shown by the strong relation between the RIV and the residency time, the latter is a good indicator to quantify the forcing exerted by the LBC on the RCM simulation. The residency time can thus be used as a tool to objectively compare the forcing from the LBC on the RCM. It could also be useful to identify the level of IV for different RCM configurations by avoiding the high-computational cost of a large ensemble of simulations.

The scatter diagram analyses also indicate that the RCM loses predictability with time for each air parcels in a similar way as a GCM, but more slowly because of the LBC forcing. Indeed, an extrapolation of the linear

fit of the scatter diagram shows that RIV for MSLP reaches a value of 1, corresponding to a complete loss of correlation between the RCM simulations, in more than 20 days of residency time. This value is larger than the approximate 14 days required for two GCM simulations to diverge completely. The fact that the RIV for PCP reaches values close to 1 faster than the other variables shows that PCP is less controlled by the LBC forcing and is more influenced by local processes than MSLP and ST. On the contrary, the extrapolation of the linear fit for the RIV of ST shows that an RIV of 1 will be reached in about 25 days, meaning that the time response of ST is longer than PCP and MSLP.

5. Conclusions

This study presents a new tool to quantify the lateral boundary forcing of regional climate model (RCM) simulations. This tool computes the residency time of the air parcels inside the limited-area domain. The method to compute the residency time consists of attributing an aging tracer of zero age to each air parcel that penetrates the limited-area domain. During the integration of a given RCM simulation, the aging tracers grow older with every time step as they migrate through the limited-area domain along the atmospheric circulation. The aging tracers are processed into the RCM dynamics, which means that they are advected and diffused following the atmospheric circulation.

The residency time computed with the aging tracer is treated and archived as any other meteorological variable simulated in the RCM, thus allowing climate diagnostics of this parameter. The residency time and the horizontal wind showed a clear annual cycle, where the residency time is generally shorter in winter than in summer because of the faster atmospheric circulation in winter. The residency time is smaller at higher levels, in agreement with the faster atmospheric circulation. Based on a 10-yr climatology, the residency time increases within the domain from west to east according to the aging of the tracer during its migration following the general westerly atmospheric circulation. For our large domain, the maximum values of residency time at 850 hPa are located on the northeast of the domain north of Québec. The residency time allows the identification of the outflow and inflow boundaries and can be useful to describe the atmospheric circulation for different time steps, seasons, domain locations, and domain sizes.

We computed the internal variability (IV) as the intermember variance, which is an estimation of the similarities between simulations of an ensemble started with different initial conditions and using the same driving field. As in Lucas-Picher et al. (2008), the IV is computed from a 10-member ensemble of 10 yr over a large domain covering North America. The IV computed with the intermember variance [referred as the absolute internal variability (AIV)] was normalized with the temporal variance to obtain the relative internal variability (RIV). This normalization removes the dependence of the IV due to the temporal variability and enhances the part of the IV associated to the decorrelation between the RCM simulations of an ensemble (Lucas-Picher et al. 2008). The AIV for MSLP and ST show a small mean annual cycle compared to the RIV, which has larger values in summer than in winter. Contrary to the AIV, the similar annual cycles between the residency time and the RIV for MSLP, ST, and PCP reveal that the RIV is linked to the atmospheric circulation. Likewise, the similarity between the spatial distribution of the RIV and the residency time shows that the normalization of the AIV with the temporal variance increases the part of the IV linked to the atmospheric circulation.

To investigate the association between the spatial distribution of the residency time, the AIV, and the RIV, we used the scatter diagram analysis. The scatter diagrams show that the AIV increases linearly with the residency time and is larger in winter than in summer for a corresponding residency time. The RIV also shows a linear relation with the residency time, but with a similar behavior in summer and in winter. This nonseasonal dependence of the relation between the RIV and the residency time refutes the earlier speculation that internal variability is larger in summer than in winter because of the convective activity and numerous nonlinear processes occurring in summer (Giorgi and Bi 2000). However, it supports the argument that internal variability is linked to the atmospheric circulation (Rinke et al. 2004; Lucas-Picher et al. 2008) and depends on the flushing regime (von Storch 2005b). With this perspective, the residency time can be considered a good quantitative indicator of the control of the LBC exerted on the RCM. It can be used as a proxy to quantify the control of the LBC on the RCM in order to compare the LBC forcing for different RCM configurations (i.e., domain sizes, domain locations and seasons). The fact that the tracer is not affected by the subgrid-scale physical parameterization (e.g., vertical transportation by the convection) could slightly influence the previous conclusions by changing the behavior of the tracer, especially in summer. This fact could explain the higher correlation coefficients observed between the RIV and the residency time in winter than in summer.

The relations and conclusions drawn from this work

were derived from an analysis using a specific experimental configuration. Although some conclusions are independent of the experimental configuration, this type of analysis should be repeated over different domain sizes and locations before generalizing the findings of this work. While the usefulness of the aging tracer was described using a climate analysis, this tracer can also be used for weather purposes such as testing the predictability of weather forecast using limited-area domains. Another interesting application of the aging tracer could be to link the spatial spinup, a minimum space required to generate the small scales in an RCM (Leduc and Laprise 2008), to a temporal spinup computed by the residency time. Finally, the residency time can be employed to quantify the forcing from the lateral boundary conditions and to objectively determine the intensity of the large-scale nudging already employed in RCM simulations integrated over large domains.

Acknowledgments. This work is part of the Ph.D. thesis of the first author in Environmental Sciences at Université du Québec à Montréal. The authors thank Claude Desrochers and Mourad Labassi for maintaining a user-friendly local computing environment at the Ouranos Consortium. The Ouranos Consortium, the Canadian Climate Variability Research Network (CLIVAR), the Natural Sciences and Engineering Research Council (NSERC), and the Canadian Foundation for Climate and Atmospheric Sciences (CFCAS) financially supported this research. Finally, the authors thank Dr. Maryse Picher for her careful revision that improved the readability of the manuscript.

REFERENCES

Alexandru, A., R. de Elía, and R. Laprise, 2007: Internal variability in regional climate downscaling at the seasonal time scale. *Mon. Wea. Rev.,* **135,** 3221–3238.

Anthes, R. A., Y. H. Kuo, D. P. Baumhefner, R. M. Errico, and T. W. Bettge, 1985: Predictability of mesoscale motions. *Advances in Geophysics,* Vol. 288, Academic Press, 159–202.

Caya, D., and R. Laprise, 1999: A semi-implicit semi-Lagrangian regional climate model: The Canadian RCM. *Mon. Wea. Rev.,* **127,** 341–362.

——, and S. Biner, 2004: Internal variability of RCM simulations over an annual cycle. *Climate Dyn.,* **22,** 33–46.

Christensen, J. H., T. R. Carter, and F. Giorgi, 2002: PRUDENCE employs new methods to assess European climate change. *Eos, Trans. Amer. Geophys. Union,* **83,** 147.

Christensen, O. B., M. A. Gaertner, J. A. Prego, and J. Polcher, 2001: IV of regional climate models. *Climate Dyn.,* **17,** 875–887.

Davies, H. C., 1976: A lateral boundary formulation for multilevel prediction models. *Quart. J. Roy. Meteor. Soc.,* **102,** 405–418.

de Elía, R., R. Laprise, and B. Denis, 2002: Forecasting skill limits of nested, limited-area models: A perfect-model approach. *Mon. Wea. Rev.,* **130,** 2006–2023.

——, and Coauthors, 2008: Evaluation of uncertainties in the CRCM-simulated North American climate. *Climate Dyn.,* **30,** 113–132, doi:10.1007/s00382-007-0288-z.

Dickinson, R. E., R. M. Errico, F. Giorgi, and G. T. Bates, 1989: A regional climate model for the western United States. *Climatic Change,* **15,** 383–422.

Gates, W. L., and Coauthors, 1999: An overview of the results of the Atmospheric Model Intercomparison Project. *Bull. Amer. Meteor. Soc.,* **80,** 29–55.

Gheusi, F., and J. Stein, 2002: Lagrangian description of airflows using Eulerian passive tracers. *Quart. J. Roy. Meteor. Soc.,* **128,** 337–360.

Giorgi, F., 1990: Simulations of regional climate using limited-models nested in a general circulation models. *J. Climate,* **3,** 941–963.

——, and X. Bi, 2000: A study of IV of regional climate model. *J. Geophys. Res.,* **105,** 29 503–29 521.

Houghton, J. T., L. G. Meira Filho, B. A. Callander, N. Harris, A. Kattenberg, and K. Maskell, Eds., 1996: *Climate Change 1995: The Science of Climate Change.* Cambridge University Press, 572 pp.

——, Y. Ding, D. J. Griggs, M. Noguer, P. J. van der Linden, X. Dai, K. Maskell, and C. A. Johnson, Eds., 2001: *Climate Change 2001: The Scientific Basis*. Cambridge University Press, 881 pp.

Jacob, D., and R. Podzun, 1997: Sensitivity studies with the regional climate model REMO. *Meteor. Atmos. Phys.,* **63,** 119–129.

Jones, R. G., J. M. Murphy, and M. Noguer, 1995: Simulation of climate change over Europe using a nested regional-climate model. I: Assessment of control climate, including sensitivity to location of lateral boundaries. *Quart. J. Roy. Meteor. Soc.,* **121,** 1413–1449.

——, ——, ——, and A. B. Keen, 1997: Simulation of climate change over Europe using a nested regional-climate model. II: Comparison of driving and regional model responses to a doubling of carbon dioxide. *Quart. J. Roy. Meteor. Soc.,* **123,** 265–292.

Kalnay, E., and Coauthors, 1996: The NCEP/NCAR 40-Year Reanalysis Project. *Bull. Amer. Meteor. Soc.,* **77,** 437–471.

Laprise, R., 2005: High-resolution climate modelling: Assessment, added value and applications—A foreword. *High-Resolution Climate Modelling: Assessment, Added Value and Applications, Extended Abstracts of a WMO/WCRP-Sponsored Regional-Scale Climate Modelling Workshop,* L. Barring and R. Laprise, Eds., Lund University, 12–16. [Available online at http://www.nateko.lu.se/ELibrary/Lerpg/5/Lerpg5Article.pdf.]

——, M. Ravi Varma, B. Denis, D. Caya, and I. Zawadzki, 2000: Predictability in a nested limited-area model. *Mon. Wea. Rev.,* **128,** 4149–4154.

Leduc, M., and R. Laprise, 2008: Regional Climate Model sensitivity to domain size. *Climate Dyn.,* doi:10.1007/s00382-008-0400-z, in press.

Lucas-Picher, P., D. Caya, R. de Elìa, and R. Laprise, 2008: Investigation of regional climate models' internal variability with a ten-member ensemble of ten years over a large domain. *Climate Dyn.*, doi:10.1007/s00382-008-0384-8, in press.

McFarlane, N. A., G. J. Boer, J. P. Blanchet, and M. Lazare, 1992: The Canadian Climate Centre second-generation general cir-

culation model and its equilibrium climate. *J. Climate,* **5,** 1013–1044.

McGregor, J. L., 1997: Regional climate modelling. *Meteor. Atmos. Phys.,* **63,** 105–117.

Mearns, L., 2004: North American Regional Climate Change Assessment Program (NARCCAP): A multiple AOGCM and RCM climate scenario project over North America. *Eos, Trans. Amer. Geophys. Union,* **85** (Fall Meeting Suppl.), Abstract A51F-02.

Miguez-Macho, G., G. L. Stenchikov, and A. Robock, 2004: Spectral nudging to eliminate the effects of domain position and geometry in regional climate model simulations. *J. Geophys. Res.,* **109,** D13104, doi:10.1029/2003JD004495.

Noguer, M., R. Jones, and J. Murphy, 1998: Sources of systematic errors in the climatology of a regional climate model. *Climate Dyn.,* **14,** 691–712.

Plummer, D. A., and Coauthors, 2006: Climate and climate change over North America as simulated by the Canadian RCM. *J. Climate,* **19,** 3112–3132.

Rinke, A., and K. Dethloff, 2000: On the sensitivity of a regional Arctic climate model to initial and boundary conditions. *Climate Res.,* **14,** 101–113.

——, P. Marbaix, and K. Dethloff, 2004: IV in Arctic regional climate simulations: Case study for the Sheba year. *Climate Res.,* **27,** 197–209.

Separovic, L., R. de Elía, and R. Laprise, 2008: Reproducible and irreproducible components in ensemble simulations with a regional climate model. *Mon. Wea. Rev.,* **136,** 4942–4961.

Solomon, S., D. Qin, M. Manning, M. Marquis, K. Averyt, M. M. B. Tignor, H. L. Miller Jr., and Z. Chen, Eds., 2007: *Climate Change 2007: The Physical Science Basis.* Cambridge University Press, 996 pp.

Takle, E., and Coauthors, 1999: Project to Intercompare Regional Climate Simulations (PIRCS): Description and initial results. *J. Geophys. Res.,* **104,** 19 443–19 461.

Tjernstrom, M., and Coauthors, 2005: Modelling the Arctic boundary layer: An evaluation of six ARCMIP regional-scale models using data from the SHEBA Project. *Bound.-Layer Meteor.,* **117,** 337–381.

Vannitsem, S., and F. Chomé, 2005: One-way nested regional climate simulations and domain size. *J. Climate,* **18,** 229–233.

Vidale, P. L., D. Lüthi, C. Frei, S. I. Seneviratne, and C. Schär, 2003: Predictability and uncertainty in a regional climate model. *J. Geophys. Res.,* **108,** 4586, doi:10.1029/2002JD002810.

von Storch, H., 2005a: Models of global and regional climate. *Encyclopedia of Hydrological Sciences, Part 3: Meteorology and Climatology,* M. G. Anderson, Ed., John Wiley and Sons, 478–490.

——, 2005b: Conceptual basis and application of regional climate modeling. *High-Resolution Climate Modelling: Assessment, Added Value and Applications, Extended Abstracts of a WMO/WCRP-Sponsored Regional-Scale Climate Modelling Workshop,* L. Barring and R. Laprise, Eds., Lund University, 26–27. [Available online at http://www.nateko.lu.se/ELibrary/Lerpg/5/Lerpg5Article.pdf.]

Weisse, R., H. Heyen, and H. von Storch, 2000: Sensitivity of a regional atmospheric model to a sea state dependent roughness and the need of ensemble calculations. *Mon. Wea. Rev.,* **128,** 3631–3642.

Wu, W., A. H. Lynch, and A. Rivers, 2005: Estimating the uncertainty in a regional climate model related to initial and lateral boundary conditions. *J. Climate,* **18,** 917–933.